www.sciencemag.org/content/363/6432/1193/suppl/DC1

# Supplementary Materials for

## The oceanic sink for anthropogenic $CO_2$ from 1994 to 2007

Nicolas Gruber*, Dominic Clement, Brendan R. Carter, Richard A. Feely, Steven van Heuven, Mario Hoppema, Masao Ishii, Robert M. Key, Alex Kozyr, Siv K. Lauvset, Claire Lo Monaco, Jeremy T. Mathis, Akihiko Murata, Are Olsen, Fiz F. Perez, Christopher L. Sabine, Toste Tanhua, Rik Wanninkhof

*Corresponding author. Email: nicolas.gruber@env.ethz.ch

Published 15 March 2019, *Science* **363**, 1193 (2019)
DOI: 10.1126/science.aau5153

**This PDF file includes:**

## Materials and Methods

Data

The main data we employ come from the merged and internally consistent GLODAPv2 data product (*8*), which consists of high-quality measurements of dissolved inorganic carbon (*DIC*), total alkalinity (*Alk*), and related parameters, such as the macronutrients nitrate, phosphate, and silicic acid, and dissolved oxygen, from a total of 724 cruises covering the global ocean and spanning the period from 1972 through 2012. This global data product was built on the basis of earlier collections, starting with the first version of GLODAP (*49*), but also including the CARINA collection in the Atlantic and Southern Ocean (*50*, *51*) and the PACIFICA collection in the Pacific (*52*). Numerous additional cruises with high quality data, particularly from the Repeat Hydrography /GO-SHIP program (*7*) were included into GLODAPv2 as well, making this the world's largest and most complete collection of interior ocean inorganic carbon data (*8*). The GLODAPv2 data underwent strict quality control procedures (i.e., bias adjustments) in order to achieve internal consistency, which is a key requirement for the analysis of long-term trends. The level of consistency of the data obtained after adjustments was determined to be better than 0.005 in salinity (S), 1% in oxygen ($O_2$), 2% in nitrate ($NO_3^-$), 2% in silicic acid ($Si(OH)_4$), 2% in phosphate ($PO_4^{3-}$), 4 μmol $kg^{-1}$ in dissolved inorganic carbon (DIC), and 6 μmol $kg^{-1}$ in total alkalinity (*Alk*).

We modified the GLODAPv2 data product in two ways. First, we added two GO-SHIP cruises in the Atlantic (A16S, 2013/2014, and A16N, 2013, https://cchdo.ucsd.edu/cruise/33RO20131223, 33RO20130803) in order to have a better temporal coverage of this basin for the Repeat Hydrography Program/GO-SHIP era (henceforth referred to as GO-SHIP era, although this era is ongoing). Second, several cruises/stations were excluded from the analyses for a number of reasons: (i) too early, i.e., all data before 1981 were excluded in order to avoid the inclusion of data with possibly enhanced measurement uncertainty and also data that require an excessive temporal adjustment, (ii) outside analysis domain, i.e., data stemming from marginal seas (Mediterranean, Sea of Japan, etc.) and north of 65°N were not considered, and (iii) not all variables needed to compute C* and to establish the linear regressions were available. The third criterion, i.e., the availability of the whole suite of variables was by far the most important exclusion criterion, as it excluded about 75% of all samples in GLODAPv2. A final manual quality control (iv) checked for stations with an excessive amount of scatter in the computed C* tracer. This affected mostly a few selected stations, primarily located in the Southern Hemisphere (Figure S1).

Given our goal to estimate decadal changes in anthropogenic carbon between the 1990s (JGOFS/WOCE era) and the 2000s and 2010s (GO-SHIP era), we assigned each cruise to one of these two eras, using January 1st, 2000 as the separation. Figure S1 depicts the resulting spatial distribution of the cruises for each of the two eras, color-coded according to the year of observation. In Figure S2, the data distribution in time is shown, color coded according to ocean basin. The overall distribution is relatively homogeneous, with the median year for all retained measurements being 1994 for the JGOFS/WOCE era and 2007 for the GO-SHIP era. Unfortunately, there are also large spatial gaps. Especially striking is the relatively poor coverage of the Indian Ocean during the GO-SHIP era up to 2012.

In order to map the estimated change in anthropogenic $CO_2$ to the global ocean, we employ two gridded products, i.e., the gridded GLODAPv2 product (*53*) for nitrate, phosphate, silicic acid, oxygen, and the apparent oxygen utilization ($AOU = O_2^{sat} - O_2$), and the gridded World Ocean Atlas 2013 (WOA) product for temperature (*54*) and salinity (*55*). Although the GLODAPv2 gridded product is based on fewer data than the WOA product, its source data is fully quality controlled and internally consistent. In contrast, the WOA product may have inherited substantial biases from its source data, which have been subject to only a minimum level of 2nd quality control. This is a particular concern for the nutrients since standard reference materials for these parameters that would allow for a more direct comparability of the different measurements have become available only very recently (*56*). An additional reason to employ the GLODAPv2 product is that it is consistent with the data that was used to determine the predictive relationships for $\Delta_t C_{ant}$. This avoids mapping biases, particularly in the deeper parts of the ocean, where small offsets can lead to substantial errors in the estimation of $\Delta_t C_{ant.}$ Since quality issues and biases are much smaller for S and T, owing to their high inherent accuracy and the well-established use of standards, we opted for the WOA product for these two parameters. In the sensitivity studies described in more detail below, we explore the impact of this data selection choice.

Determination of change in anthropogenic $CO_2$:

We determine the change in the oceanic anthropogenic $CO_2$ concentration between the two eras by employing the recently developed eMLR(C*) method (*9*). This method builds on the well-established eMLR method (*10*, *57*), but extends it in several ways to deal primarily with (i) the temporal inhomogeneity of the data and (ii) with the spatial inhomogeneity of the observations, i.e., the fact that only a subset of the cruises represent repeat occupations of the same lines. The eMLR(C*) method employs a probabilistic approach in the selection of the independent variables for the eMLR, thereby avoiding many of the problems associated with the choice of variables when building regression models (*43*, *58*). A full description of the method including a detailed assessment of its performance on the basis of synthetic data from a hindcast simulation with an ocean biogeochemical model is given in ref (*9*). Here, we provide a brief description including the specific modifications undertaken to deal with real observations.

The method proceeds in three steps (Figure S3). In the first step, the semi-conservative tracer $C^* = DIC - r_{C:P}\, PO_4^{3-} - 1/2\, (Alk + r_{N:P}\, PO_4^{3-})$ (*45*, *59*) is computed from the measured *DIC*, *Alk* and phosphate ($PO_4^{3-}$) assuming a constant stoichiometric C:P and N:P ratio during photosynthesis and respiration/remineralization ($r_{C:P}$ = 116:1, $r_{N:P}$ = 16:1). We use here phosphate instead of nitrate in order to avoid issues with denitrification (*59*), even though the relative measurement precision is better for nitrate than for phosphate. If the assumption of constant stoichiometric ratios is correct, then the spatio-temporal distribution of C* reflects only the effect of the exchange of natural and anthropogenic $CO_2$ across the air-sea interface on the observed DIC (*6*). This strongly enhances the interpretability of the signals - an advantage that largely persists even when considering the fact that the stoichiometric ratios $r_{C:P}$ and $r_{N:P}$ are likely variable (*60*). A corollary advantage of using *C** in the eMLR method compared to the commonly used *DIC* (*30*, *43*, *61*) is the smaller variance in *C**, permitting us to develop more accurate statistical models (*9*).

In the second step, the $C^*$ values for each observational era are normalized to the median for the respective periods (1994 for JGOFS/WOCE and 2007 for GO-SHIP). This normalization is achieved by assuming a transient steady state (*27*), which applies strictly for linear systems that are exponentially forced for an amount of time that is longer than the adjustment time– a condition that is largely met by the ocean carbon uptake (*28*) (see below for a more thorough discussion). This assumption predicts that in an ocean with time-constant circulation and mixing, the change in anthropogenic $CO_2$ burden between two years is proportional to the amount of anthropogenic $CO_2$ that is already present, with the proportionality determined by the relative change in atmospheric $CO_2$ between these two years (*28*), i.e., $C^*(t^{ref}) = C^*(t) - \beta(t) \cdot C_{ant}(t^{ref})$, with $\beta(t) = (CO_2^{atm}(t) - CO_2^{atm}(t^{ref}))/(CO_2^{atm}(t^{ref}) - CO_2^{atm}(t^{pi}))$[1], where $t^{ref}$ is the reference year, $t^{pi}$ is the preindustrial time and $t$ is the year the measurement was taken. We use the global mean atmospheric $CO_2$ from ref (*37*) for $CO_2^{atm}$ at times $t$ and $t^{ref}$, and a value of 280 ppmv for atmospheric $CO_2$ at preindustrial time, i.e., $CO_2^{atm}(t^{pi})$. For the JGOFS/WOCE period, $t_1^{ref}$, we use for $C_{ant}(t_1^{ref})$ the globally gridded estimate of Sabine et al. (*49*). For the GO-SHIP period, $t_2^{ref}$, we constructed a corresponding distribution for $C_{ant}(t_2^{ref})$ from $C_{ant}(t_1^{ref})$ using the same transient steady state assumption, i.e., we scaled up the estimates for 1994 to 2007 using $\alpha$=0.28 (see below for detailed justification). Since the majority of the measurements were taken relatively close in time to the two reference years, these adjustments are usually less than 2 to 3 µmol $kg^{-1}$. As a result, the sensitivity of the final results to these choices is very small (see ref (*9*)).

In the third step, the adjusted data from the two observational eras are fitted with multiple linear regressions. To this end, we binned the data into ranges of neutral density, i.e., isoneutral slabs: 14 for the Atlantic and 12 for the combined Indo-Pacific ocean basins (Table S1). Data above 150 m were excluded from the fit in order to avoid the inclusion of seasonal biases. The $C^*$ observations for each of the 26 slabs from the JGOFS/WOCE period ($t_1^{ref}$) were then fitted with linear functions of the form: $C^*(t_1^{ref}) = a_{1,0} + \sum a_{1,i} \cdot T_i(t_1) + residual(t_1)$, where $a_{1,0}$ and $a_{1,i}$ are the coefficients of the linear fit, $T_i(t_1)$ are the $i$ independent, co-measured variables used as predictors. The same procedure was completed for the data from the GO-SHIP period ($t_2^{ref}$), i.e., $C^*(t_2^{ref}) = a_{2,0} + \sum a_{2,i} \cdot T_i(t_2) + residual(t_2)$. The coefficients of the two fits are then combined to form the eMLR-based estimate of the change in anthropogenic $CO_2$ between the two reference periods, i.e., $\Delta C_{ant}(t_2^{ref}-t_1^{ref}) = (a_{2,0} - a_{1,0}) + \sum (a_{2,i}-a_{1,i}) \cdot T_i^{clim}$, where $T_i^{clim}$ is the climatological distribution of the independent tracer $T_i$. We use a probabilistic approach in our selection of the independent variables (see also ref (*43*)). For each isoneutral slab and ocean basin, we first fit all possible combinations of the following 7 independent variables: temperature, salinity, phosphate, silicic acid, $PO_4^* = PO_4 - 16 \cdot NO_3 + 2.9$ (*62*), oxygen, and *AOU* under the constraint that a minimum of two, but not more than 5 independent tracers are selected. This gives a total of 112 combinations. Out of these combinations, the 10 best fits are selected for each subset, with the quality of the fit determined from the combined root mean square error (RMSE) of both survey periods. Each of these 10 best fits are then combined with the climatological fields of the independent tracers $T_i^{clim}$, to estimate the change in anthropogenic $CO_2$ throughout the global ocean.

[1] Please note that the corresponding equation (6) in ref(*9*) is missing the $CO_2^{atm}(t^{pi})$ term in denominator. This is a mistake and a correction will be submitted to the journal.

We employ two methods to estimate the change in the anthropogenic $CO_2$ in the top 150 m. For waters with a neutral density higher than 26.0 kg $m^{-3}$, i.e., for the isoneutral slabs outcropping at temperate latitudes and higher, we extrapolate the eMLR equations from the ocean interior of that slab all the way to the surface. For the lower densities, we employ the transient equilibrium approach (*63*), i.e., we make the well-tested assumption that the $CO_2$ system in these waters has followed the increase in atmospheric $CO_2$ closely (*11*). This permits us to compute the change in anthropogenic $CO_2$ directly from the change in atmospheric $CO_2$ using thermodynamic considerations only. Specifically, we use eq 10.2.16 in ref (*11*) to estimate the change in anthropogenic $CO_2$ in the upper ocean by computing $\Delta_t C_{ant}^{eq}(t_2^{ref} - t_1^{ref}) = 1/\gamma \cdot DIC/pCO_2 \cdot (pCO_2^{atm}(t_2^{ref}) - pCO_2^{atm}(t_1^{ref}))$, where *DIC* and $pCO_2$ are the in situ values, where $\gamma$ is the buffer (Revelle) factor and where we evaluated the right-hand side using CO2SYS(*64*) employing the Mehrbach constants(*65*) as refitted by Dickson and Millero(*66*) using the climatological values for temperature, salinity, *DIC* and *Alk*.

Calculations of changes in the column inventory of anthropogenic $CO_2$:

To compute the changes in the column inventory of anthropogenic $CO_2$, any negative values are set to zero and the resulting non-negative values are then integrated from the surface down to 3000 m. We do not integrate to greater depth, as we consider the reconstruction to be too uncertain there. In addition, we expect only a very small fraction of the total increase in the oceanic burden of anthropogenic $CO_2$ to accumulate below 3000 m since model simulations, as well as the total anthropogenic $CO_2$ burden from the pre-industrial to the 1994 (*1*), suggest that this fraction is substantially less than 5%. Nevertheless, we added 1 Pg C to the inventory of the Atlantic (0.7 Pg C in the North Atlantic, and the remaining 0.3 Pg C in the South Atlantic) to account for the contribution of the waters below 3000 m. This number as well as its distribution is largely based on the fraction of uptake into these waters that occurred between the preindustrial and 1994(*1*).

We also take into account the increase in anthropogenic $CO_2$ in regions not covered by our method, i.e., the Arctic, the Nordic Seas (north of 65°N) and the Mediterranean. (Note that our estimate covers the other marginal seas, namely the Caribbean, the Gulf of Mexico, and the Sea of Japan). To account for the contribution of these unmapped regions, we use independent estimates of the anthropogenic $CO_2$ accumulation in these regions. The majority of these estimates concern the total inventory, making it necessary to scale them to the time period of interest here, i.e., 1994 through 2007. To this end, we apply again the transient steady state assumption, and scale the inventories with a scaling factor $\alpha$=0.28 (see below). We also use this assumption to correct the reported inventories back to the same starting year, i.e., 1994. This yields, for the Arctic, starting from the reported range of inventory of between 2.5 to 3.3 Pg C for 2005(*23*) an expected change of 0.6 to 0.9 Pg C between 1994 and 2007. For the Nordic Seas, we infer an increase of 0.2 to 0.4 Pg C, based on an inventory estimate of 0.9 to 1.4 Pg for 2002(*22*). For the Mediterranean, the corresponding estimate is 0.3 to 0.6 Pg C, computed from the reported inventory of 1.3 to 2.1 Pg C for 2001(*24*). In total, we estimate that we need to add between 1.2 and 1.9 Pg C (central estimate: 1.5 Pg C) to our mapped estimate to obtain the global change in the oceanic inventory of anthropogenic $CO_2$ between 1994 and 2007.

Uncertainties:

Using synthetic data from a hindcast simulation with the NCAR CCSM model, Clement and Gruber (*9*) investigated in detail the major sources of errors and uncertainties in the reconstructed $\Delta_t C_{ant}$ fields. While the eMLR(C*) method was found to perform very well with a near zero global bias, some persistent biases were found at the basin-scale and sub-basin scale level. The tests with the model revealed that the major cause for these biases are changes in ocean circulation whose impact on the accumulation on $C_{ant}$ are not fully captured by the eMLR(C*) method (*9*). In contrast, the very skewed sampling in time and space, the assumption about transient steady state, and many other challenges mattered much less. These biases induced by circulation variability need to be taken carefully into account when interpreting the anomalous changes in $\Delta_t C_{ant}$.

To assign uncertainties to our reconstructed $\Delta_t C_{ant}$, we use two complementary approaches, each of which addresses a different aspect of uncertainty. The first approach attempts to propagate the uncertainties associated with the variable selection for the multiple linear regression models forward to the final estimated change in anthropogenic $CO_2$. This addresses one of the most important contributions to random uncertainty within the approach (cf. (*9*)). To this end, we employ a Monte Carlo method, where we select for each realization one member randomly from the 10 best regression models for each subsettted region and isoneutral slab and estimate the change in anthropogenic $CO_2$ for that model set. This procedure is repeated 100 times, yielding 100 spatial distributions of the change in anthropogenic $CO_2$ across the global ocean. We then use the standard deviation of these estimates as a measure of the random uncertainty.

In the second approach, we attempt to assess the potential impact on $\Delta_t C_{ant}$ of the subjective choices in the estimation procedure on the reconstructed change in anthropogenic $CO_2$. To this end, we used an ensemble of sensitivity analyses, wherein we made alternative choices along the three-step procedure visualized in Figure S3. Specifically, we altered (i) the climatological data the eMLR coefficients were applied on to estimate $\Delta_t C_{ant}$ globally (V102), (ii) the set of variables used to fit $C^*$ (V103 and 106), (iii) the number and distribution of regions used to subset the data (V104, V105, V107), (iv) the number of isoneutral slabs considered in the vertical subsetting (V109 and V110), (v) the data employed to determine $C^*$ (V108: no A16 cruise, and V114: all GLODAPv2 data used, i.e., no application of the exclusion criteria described above), (vi) how $\Delta_t C_{ant}$ is estimated in the upper 150 m of the water column (V111 and V112), and (vii) how $C^*$ is defined (V113). Table S2 provides a detailed description of the standard estimate (V101) and of the 13 sensitivity cases considered. We use the interquartile range (IQR) of the 14 cases as an estimate of the systematic uncertainty associated with the reconstructed change in anthropogenic $CO_2$.

Table S3 lists the reconstructed changes in anthropogenic $CO_2$ between 1994 and 2007 for the standard case as well as for each of the 13 sensitivity cases. The median column inventories differ little from the "best" estimate provided by the standard case. Figure S4 shows the corresponding column inventories and Figure S5 the contribution of the different ocean basins to the global total.

The final uncertainty in inventory is estimated by taking the square root of the sum of squared uncertainties from both the Monte Carlo and the ensemble-based estimates, where we multiplied in both cases the uncertainties first by two, i.e., we used twice the

IQR and twice the standard deviation to allow for unrecognized uncertainties. For all regions, the total uncertainty is dominated by the uncertainty stemming from the ensembles, while the contribution of the Monte Carlo based estimates is rather small.

**Supplementary Text**

Comparison with regional estimates:

The eMLR(C*)-based estimates of $\Delta_t C_{ant}$ compare overall well with the regional data-based analyses along the cruise transects conducted so far, both in terms of the vertical distributions and the column inventories. The estimated inventory change between 1990 and 2010 reported for the Pacific Ocean on the basis of a small subset of cruises(*43*) is equivalent to a mean storage rate of 0.8±0.2 Pg C $yr^{-1}$ over the 1994 to 2007 period, statistically indistinguishable from ours (1.0±0.1 Pg C $yr^{-1}$). A similar conclusion is reached in the Atlantic, where the extrapolation of four repeated cruise tracks(*61*) yields a storage rate of 0.6±0.1 Pg C $yr^{-1}$, which is somewhat smaller than ours (0.9±0.1 Pg C $yr^{-1}$). A recent North Atlantic estimate(*31*) of 0.39 Pg C $yr^{-1}$ (north of 25°N including the Arctic) is nearly identical to our estimate of 0.38±0.03 Pg C $yr^{-1}$ in the same region.

There is less agreement with the only other global attempt to estimate the change in ocean carbon storage based on DIC data so far(*67*). This study, which is based on an extrapolation of the changes in DIC diagnosed at a few locations around the world, suggested substantially larger changes in ocean storage (2.9 to 3.4 Pg C $yr^{-1}$) than our value of 2.5±0.3 Pg C $yr^{-1}$. However, given the limited dataset used in the former global estimate, its sampling bias and associated extrapolation uncertainties may explain the difference. In contrast, our data-based storage rates for the period 1994 to 2007 are in good agreement with those recently inferred from a diagnostic model of the ocean circulation, where the circulation pattern was analysed separately for the 1990s and the first decade of the 2000(*21*) (Figure S6).

Estimating the scaling factor:

We employ the transient steady-state model(*27*) to estimate the expected change in the oceanic storage of anthropogenic $CO_2$ between two time points ($t_1$ and $t_2$). This model predicts a linear proportionality between this change, $\Delta_t C_{ant}(t_2\text{-}t_1)$, and the amount of anthropogenic $CO_2$ already present in the water column at time $t_1$, $C_{ant}(t_1)$, with a proportionality factor, $\alpha$, i.e., $\Delta_t C_{ant}(t_2\text{-}t_1) \approx \alpha \cdot C_{ant}(t_1)$.

The transient steady-state model is applicable if two conditions are met: (i) The forcing has to be exponential with a constant growth rate, and (ii) the time period of interest is far along into the perturbation such that the contribution of the initial conditions has become negligible. In the case of the oceanic uptake of anthropogenic $CO_2$, the second condition is clearly met, while this is only partially the case for the first one. This is due to atmospheric $CO_2$ having nearly doubled its exponential growth rate around the middle of last century, with the exponential rate $\lambda$ having increased from about 0.01 $yr^{-1}$ to about 0.02 $yr^{-1}$. Since it takes about $1/\lambda \approx 50$ y for a system to reach the new transient steady state, this condition is just barely met for the 1994 to 2007 period. Thus, we consider the transient steady-state model as an appropriate approach to estimate the expected change in storage, but recognize that we are somewhat fortunate, since this approach would have been problematic if we had tried to apply it to an earlier period.

We estimate the proportionality factor from the relative change in atmospheric $CO_2$, taking into consideration the change in the surface ocean buffer (Revelle) factor(*68*) and the presence of a growing air-sea disequilibrium(*45*, *69*), which reflects the fact that the surface ocean is closely but not completely following the atmospheric perturbation. The derivation starts with the change in surface ocean *DIC*, i.e., $\Delta_t C_{ant}$ , driven by the increase in atmospheric $CO_2$. Using the same equation as above for $\Delta_t C_{ant}^{eq}$, but extending it to include the presence of a disequilibrium gives:

$\Delta_t C_{ant}(t_2\text{-}t_1) \approx 1/\gamma(t_1..t_2)\ DIC/pCO_2 \cdot \Delta_t pCO_2^{atm}(t_2\text{-}t_1) \cdot \xi(t_1..t_2)$,

where the disequilibrium ratio $\xi$ is the ratio of the change in the oceanic $pCO_2$, $\Delta_t pCO_2(t_2\text{-}t_1)$ over that in the atmosphere, $\Delta_t pCO_2^{atm}(t_2\text{-}t_1)$. For the Revelle factor $\gamma(t_1..t_2)$, we use its average over the period $t_1$ to $t_2$. The scaling factor $\alpha$ can then be estimated from the ratio of the changes between two time periods:

$\alpha = \Delta_t pCO_2^{atm}(t_2\text{-}t_1)/\Delta_t pCO_2^{atm}(t_0\text{-}t_1) \cdot \xi(t_1..t_2)/\xi(t_0..t_1) \cdot \gamma(t_0..t_1)/\gamma(t_1..t_2)$.

Thus, $\alpha$ depends primarily on the ratio of the change in atmospheric $CO_2$, but is modified by the changes in the buffer factor and the changes in the disequilibrium.

For the period $t_1$ = t(1994) to $t_2$ = t(2007) relative to the preindustrial $t_0$ = t(1750), the ratio of the changes in atmospheric $pCO_2$ is 0.32 ($t_0$ = 280 ppm, $t_1$ = 358 ppm, $t_2$ = 383 ppm)(*37*) with a very small uncertainty of about ±0.01. The buffer factor $\gamma$ varies strongly with the seawater chemistry, namely the ratio of DIC and Alk(*11*), but it turns out that the ratio of its changes varies very little between different water masses. Taking the buffer factor for 1950 for $\gamma(t_0..t_1)$ and that for 2000 for $\gamma(t_1..t_2)$ yields a ratio $\gamma(t_0..t_1)/\gamma(t_1..t_2)$ of 0.94 for the mean ocean and low latitude ocean, and a ratio of 0.92 for the high latitude ocean. These buffer factors were computed by using the $CO_2$ chemistry software package CO2SYS(*64*) and inputting mean surface ocean properties for ~1994(*11*), and scaled DIC values for the respective years. The uncertainty of the computation of the buffer factors is very low, but given their variability in time and space, we assign an uncertainty of ±0.02 to the ratio $\gamma(t_0..t_1)/\gamma(t_1..t_2)$. Assuming a change in the disequilibrium of about 6 µatm between the preindustrial and 1994 and about 3 µatm between 1994 and 2007 yields a ratio $\xi(t_1..t_2)/\xi(t_0..t_1)$ of 0.94. This ratio is rather sensitive to the exact choices of the not well constrained disequilibria, so that we assign it an uncertainty of ±0.05. Using this value plus the buffer factor ratio for the high latitudes and the atmospheric $pCO_2$ change ratio gives then for $\alpha$ a value of 0.28±0.02 with the majority of the uncertainty stemming from the disequilibrium ratio. Figures S7 and S8 show that the main pattern of anomalous storage are not affected by the uncertainty of the scaling factor, i.e., $\alpha$ = 0.26 yields very similar results as $\alpha$ = 0.30. Also the very small spatial variability of $\alpha$ matters little, since this leads to only very small errors in the anomalous change in $C_{ant}$, $\Delta_t C_{ant}^{anom}$ (Figure S9). Finally, Figure S10 also reveals that using an alternative estimate for the anthropogenic $CO_2$ storage in 1994, i.e., by using the ocean inversion based estimate of ref (*14*) instead of the C*-based estimate by ref (*1*) has a relatively small impact on the estimated large-scale distribution of $\Delta_t C_{ant}^{anom}$. The same conclusion applies when the expected change in anthropogenic $CO_2$ is directly taken from the ocean inversion model rather than estimated by scaling the 1994 result (compare panels c and d in Figure S10).

Estimating the anomalous outgassing of natural $CO_2$:

We use the surface ocean $pCO_2$-based air-sea $CO_2$ flux estimate of ref (*39*) for the period 1994 through 2007 and added a steady-state outgassing of river derived $CO_2$ of

0.65 Pg C $yr^{-1}$ (average of refs *70*, *71*) in order to obtain the net ocean uptake flux for this period. This estimate includes the both the uptake of anthropogenic $CO_2$ from the atmosphere as well as any anomalous outgassing of natural $CO_2$. We then used two approaches to isolate the latter.

In the first approach, we used this adjusted $CO_2$ flux in 1994, assumed that it constitutes only the anthropogenic $CO_2$ uptake flux, and then scaled it forward in time using the transient steady-state scaling used above based on atmospheric $CO_2$ in order to obtain a timeseries of the expected anthropogenic $CO_2$ uptake flux. In the second approach, we used the estimated anthropogenic uptake flux from the ocean inversion of ref(*17*) for the year 2000 and also used the transient steady-state scaling to scale it forward and backward to obtain a full timeseries of the anthropogenic uptake flux. The anomalous outgassing of flux of natural $CO_2$ was then computed by subtracting these two expected anthropogenic $CO_2$ uptake fluxes from the net uptake flux. These two approaches yielded nearly identical integrated losses of natural of $CO_2$ of 5±3 Pg C for the period 1994 until 2007. We assign an uncertainty of ±60% to this value given the large number of assumptions that go into this estimate. The most important source of uncertainty in the first approach is the assumption that the anomalous flux of natural $CO_2$ is zero in 1994, while the largest source of uncertainty for the second approach is the magnitude of the river-derived $CO_2$ outgassing.

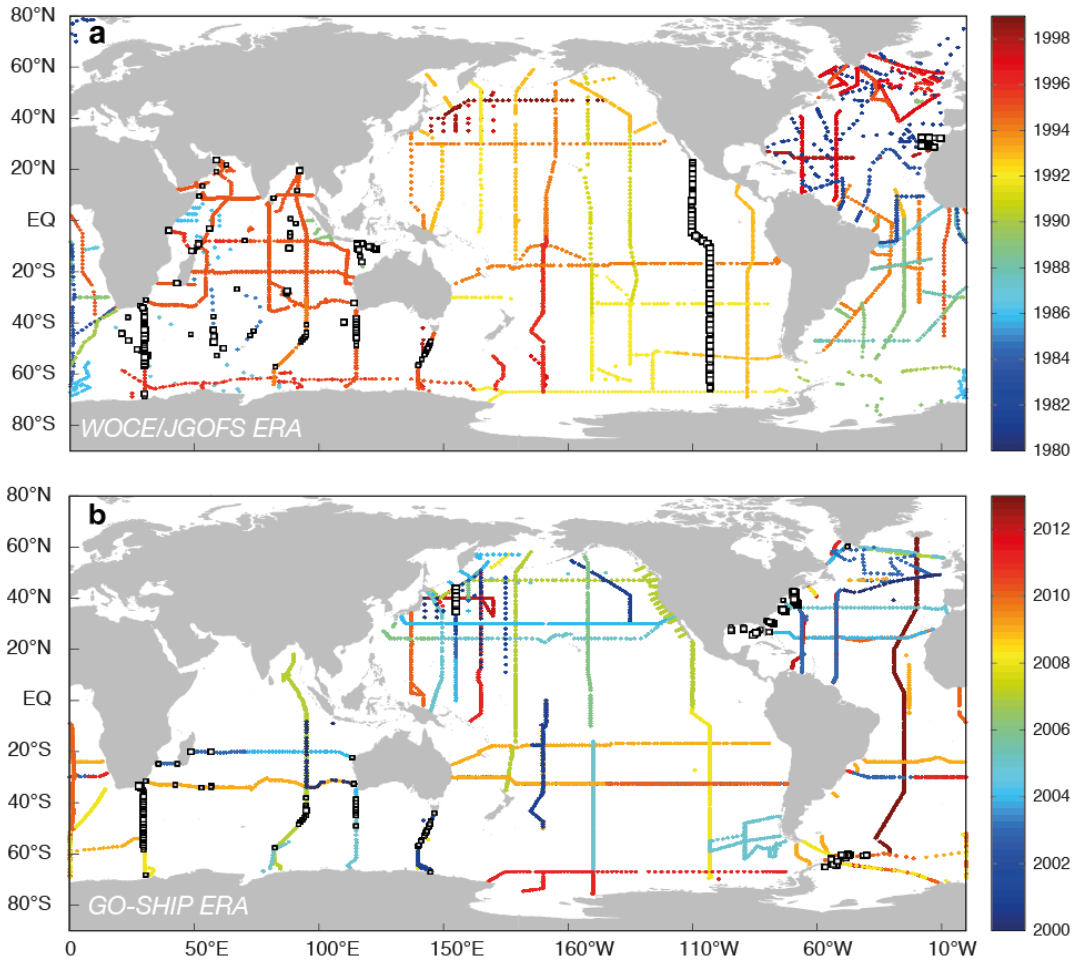


**Fig. S1.**

Maps of the sampling locations of the data used for the two eras: (a) for the WOCE/JGOFS era (1982 to 1999) and (b) as (a), but for the Repeat Hydrography/GO-SHIP era (from 2000 to 2013). The colors of the filled dots indicate the year of sampling. Open squares indicate stations/cruises that are in GLODAPv2, but not used for our analyses (see text for details). The size of the squares indicates the number of samples affected: Small: 0-9 samples, Medium: 10-19 samples, Large >19 samples. Stations that were sampled more than once during the Repeat Hydrography/GO-SHIP era are shown with two colors and with the second occupation plotted on top.

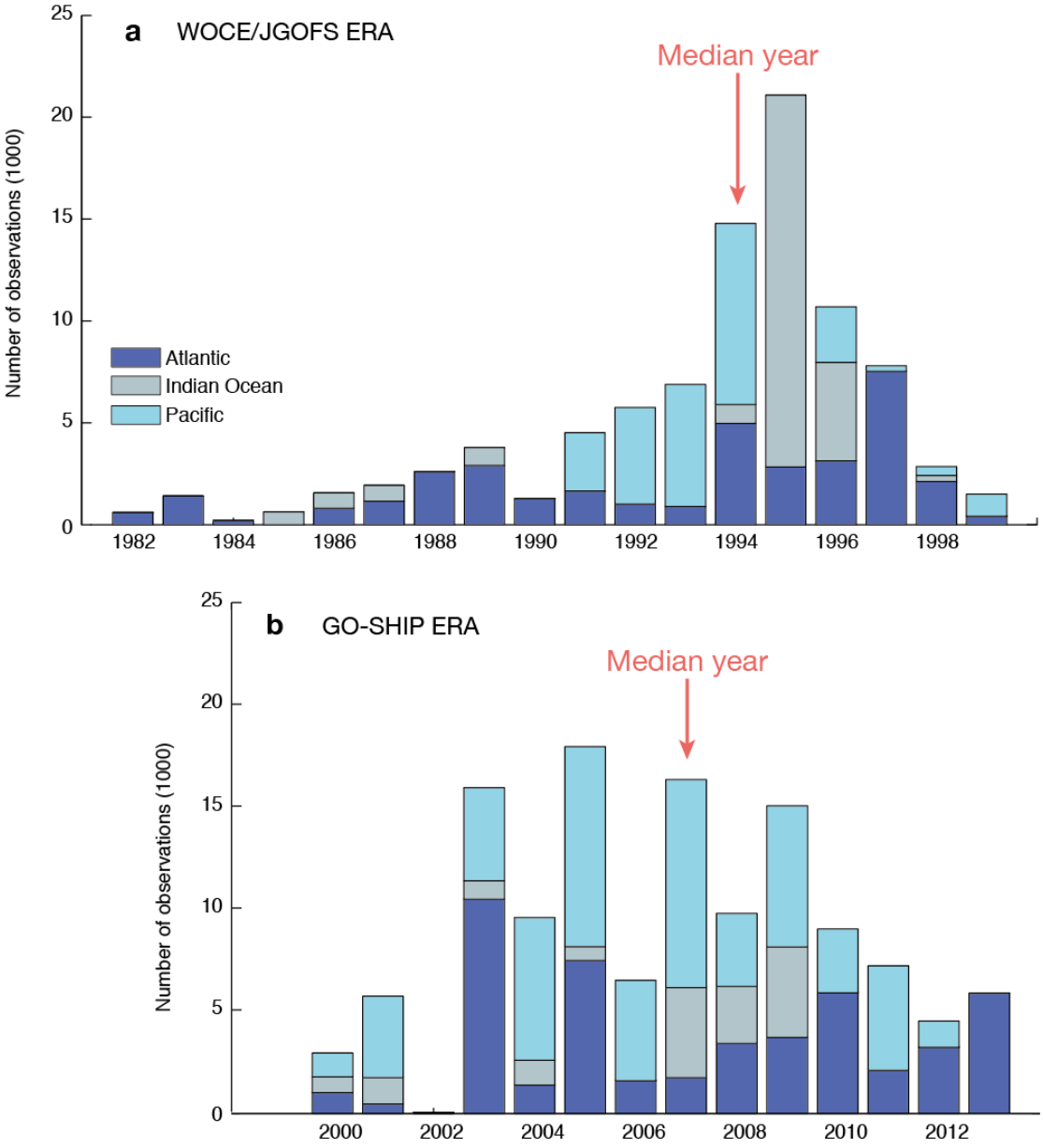


**Fig. S2.**

Distribution of the data through time. Shown are the number of discrete samples of C* for each year and basin that were used to construct the two multiple linear regression models.

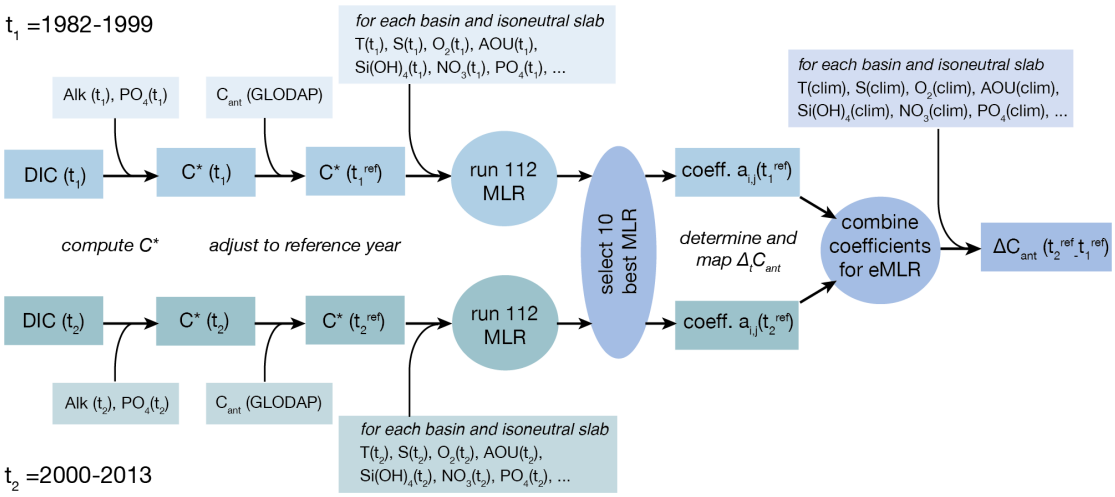


**Fig. S3.**

Procedure to estimate the change in anthropogenic $CO_2$ between the JGOFS/WOCE and the GOSHIP eras in the water column below 150 m. Adapted from ref (*9*).

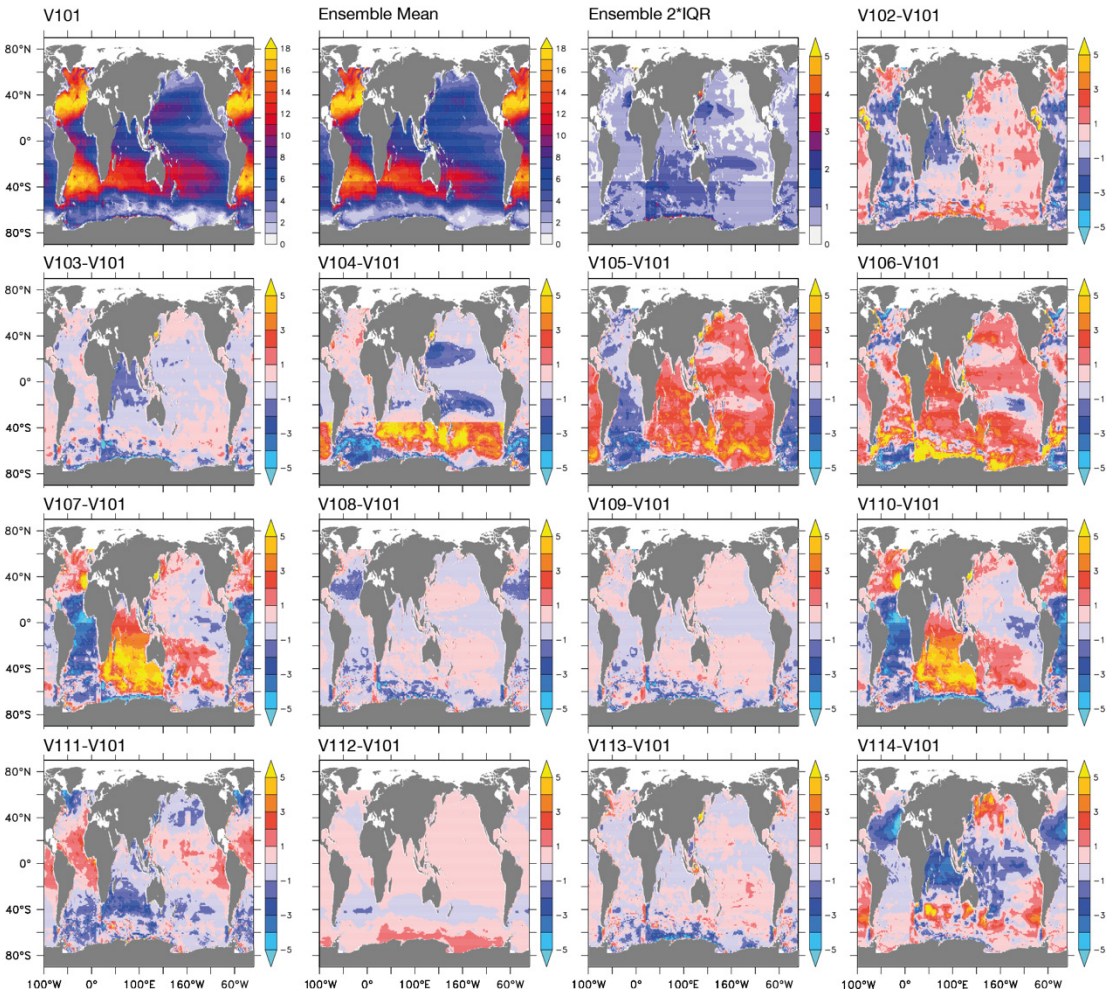


**Fig. S4.**

Column inventories of the change in anthropogenic $CO_2$ (mol $m^{-2}$) (0-3000 m) between 1994 and 2007 of the standard case and of the 13 sensitivity cases considered. Also shown are the ensemble mean of the 14 cases and twice their interquartile range. For V102 through V114, the difference to the standard case V101 is shown. (See Table S1 for a full description of these sensitivity cases).

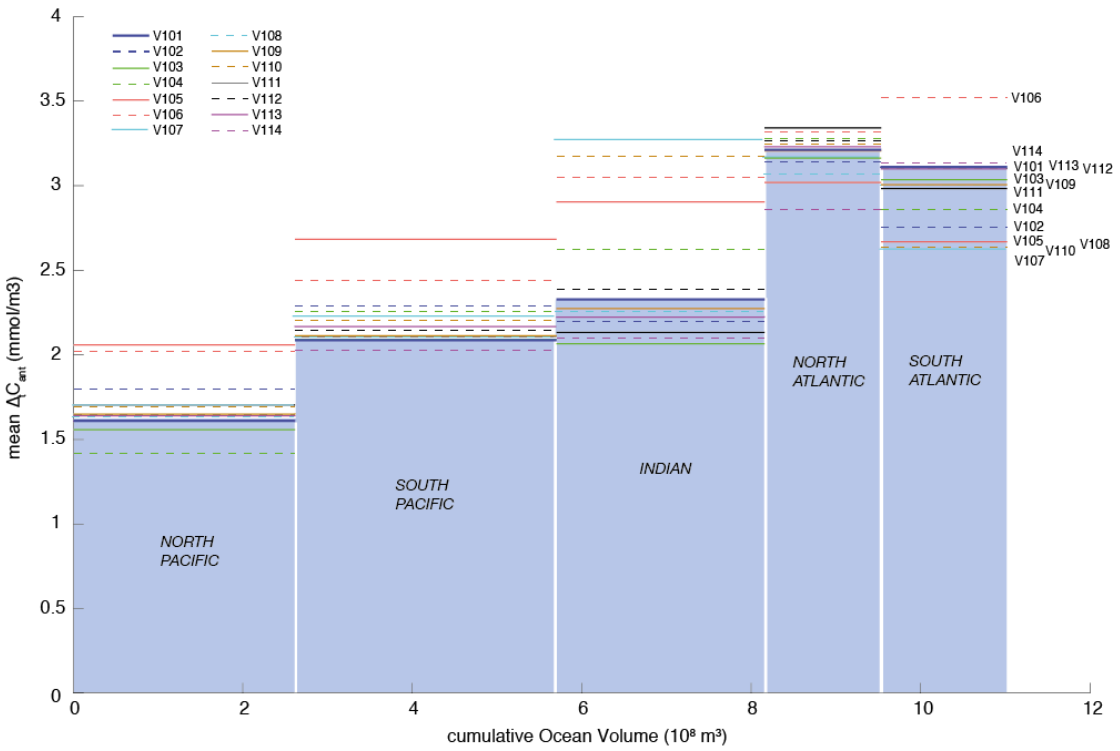


**Fig. S5.**

Inventories (0-3000 m) for the standard case as well as for the 13 sensitivity cases considered. Shown is the mean change in the concentration of anthropogenic $CO_2$ in the respective ocean basins as a function of the ocean volume. Thus, the area of the rectangle for each ocean basin is directly proportional to the total inventory change for this ocean basin.

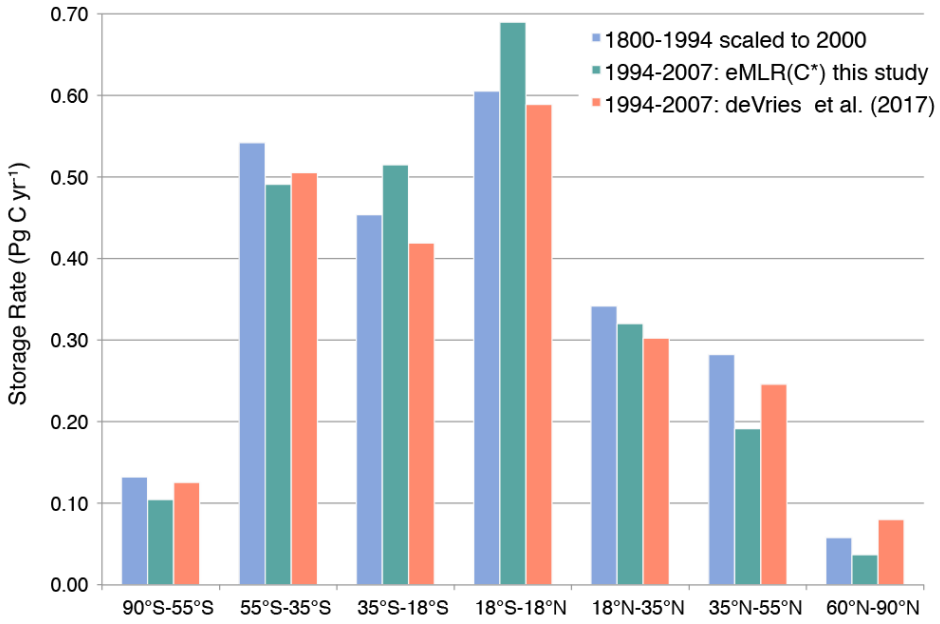


**Fig. S6.**

Comparison of the mean storage rate of anthropogenic $CO_2$ between 1994 and 2007 for the global ocean w/o the Arctic Ocean and the Mediterranean Sea. Shown are three estimates: The C* method-based estimate for the period 1800 to 1994(*1*) scaled to 2000 (blue) (see text), the eMLR(C*) based estimate (green), and a diagnostic model-based estimate(*21*), the latter interpolated to the 1994 to 2007 period. The uncertainties of the C*-based estimates are about 20%, those of the eMLR(C*) based estimates about ±10%, and those for the diagnostic model are reported to be less than 5%(*21*).

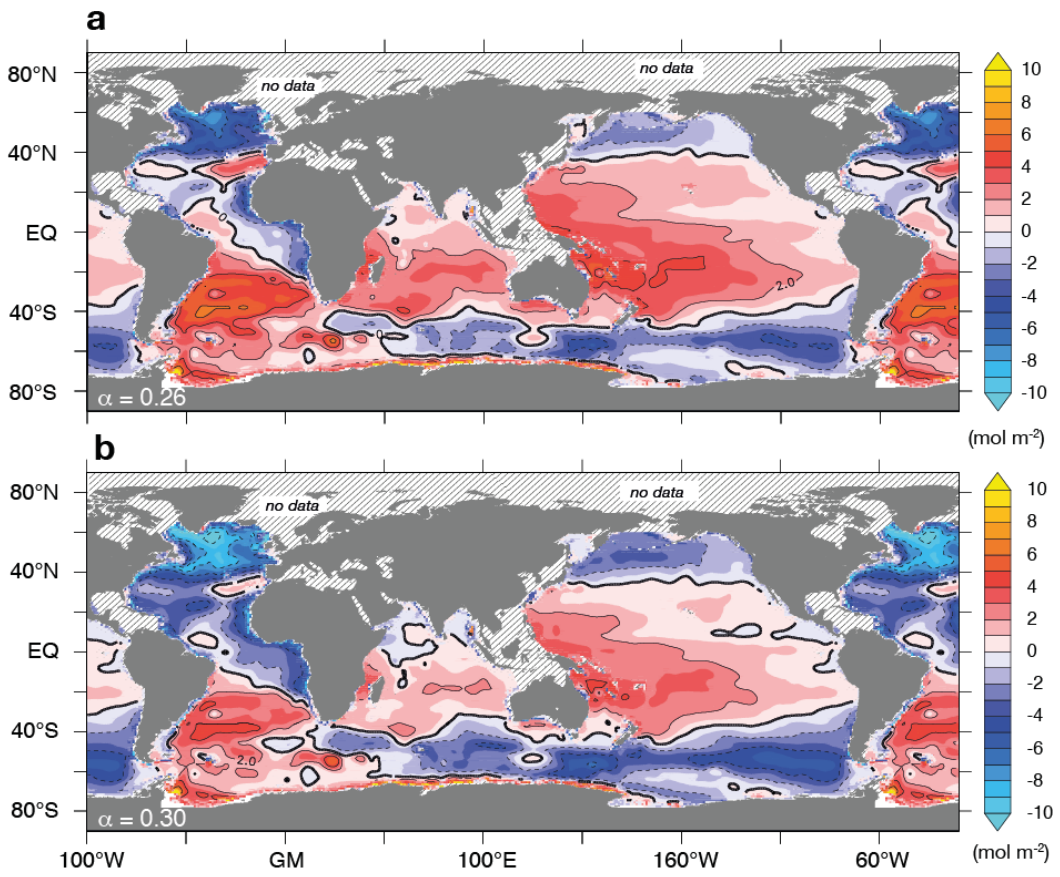


**Fig. S7.**

Sensitivity of anomalous change in storage to the value of the scaling factor α: (a) α = 0.26 (lower bound estimate), and (b) α = 0.30 (upper bound estimate).

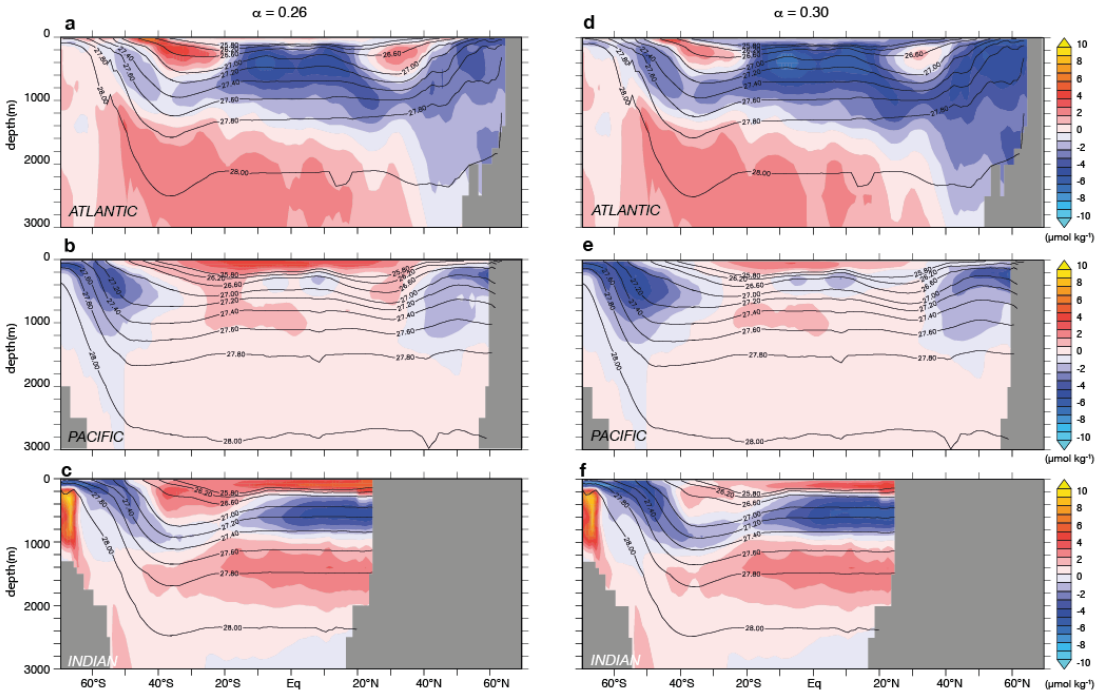


**Fig. S8.**

Sensitivity of anomalous change in the zonal mean sections of $\Delta_t C_{ant}$ to the value of the scaling factor $\alpha$: (a-c) $\alpha = 0.26$ (lower bound estimate), and (d-f) $\alpha = 0.30$ (upper bound estimate). (a, b): Atlantic Ocean, (b,e): Pacific Ocean, and (c,f): Indian Ocean..

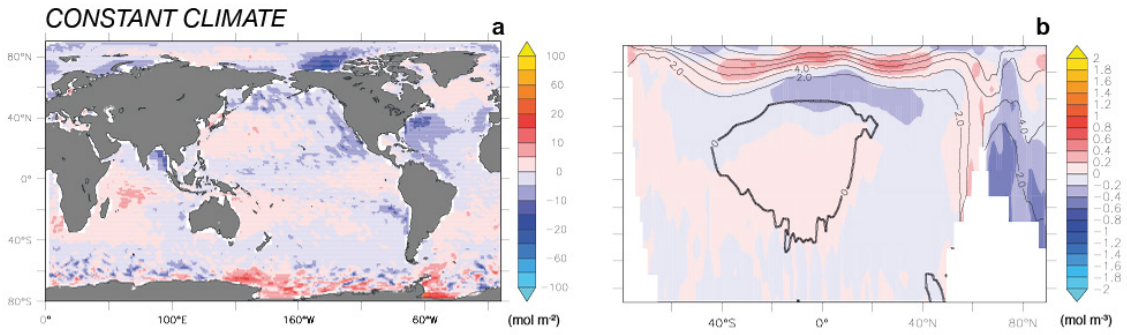


**Fig. S9.**

Assessment of the impact of the spatial variations in the scaling factor α on the estimated $\Delta_t C_{ant}^{anom}$. (a) Column inventory of the error in $\Delta_t C_{ant}^{anom}$, and (b) zonal mean section of the error in $\Delta_t C_{ant}^{anom}$. The anomalous change in both panels was computed assuming a constant scaling factor α of 0.25, i.e., $\Delta_t C_{ant}^{anom} = \Delta_t C_{ant} - 0.25 \cdot C_{ant}(1994)$ using the constant climate results from the hindcast simulations with the NCAR CCSM described in detail in (*9*).

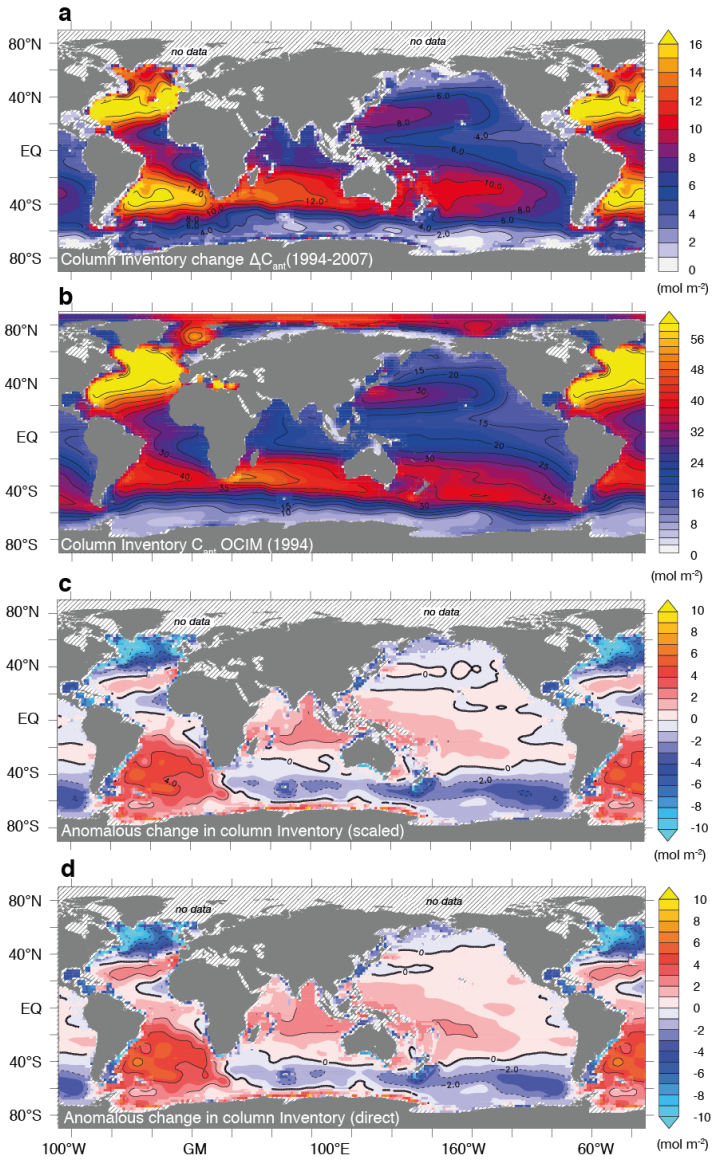


**Fig. S10.**

As Figure 3 in the main text, except for panel b showing the ocean inversion-based (OCIM) carbon inventory of anthropogenic $CO_2$ for the year 1994 from ref (*14*) instead of the C*-based estimate from ref (*1*), and panel c showing the anomalous change in $\Delta_tC_{ant}$ computed by subtracting the OCIM inventory for 1994 instead of the C*-based one, i.e, $\Delta_tC_{ant}^{anom}$(scaled) = $\Delta_tC_{ant}$(eMLR, 1994-2007) – 0.28*$C_{ant}$(OCIM, 1994). The additional panel d shows the anomalous change in $\Delta_tC_{ant}$ when the expected change in $\Delta_tC_{ant}$ between 1994 and 2007 is taken directly from the OCIM simulated change, i.e., $\Delta_tC_{ant}^{anom}$(direct) = $\Delta_tC_{ant}$(eMLR, 1994-2007) – $\Delta_tC_{ant}$(OCIM, 1994-2007). To compute $\Delta_tC_{ant}^{anom}$ for the OCIM-based estimates, the $\Delta_tC_{ant}$ estimates were interpolated onto the 2°x2° of the OCIM estimates. The similarity of panels c and d with panel c of Figure 3 in the main text indicates that $\Delta_tC_{ant}^{anom}$ is neither sensitive to the choice of the $C_{ant}$ fields for 1994 nor to the assumption of a constant scaling factor $\alpha$=0.28.

**Table S1.**

Neutral density slabs used for the eMLR(C*) method to determine the change in anthropogenic $CO_2$ and selection of predictors in the multiple linear regressions (MLR)[a]:

| Isoneutral range | Temp. | Sal. | *AOU* | $PO_4^{3-}$ | $NO_3^-$ | $Si(OH)_4$ | $PO_4$* |
|---|---|---|---|---|---|---|---|
| *Atlantic density intervals* | | | | | | | |
| <26.00 | 8 | 5 | 7 | 6 | 2 | 5 | 7 |
| 26.00-26.50 | 7 | 8 | 6 | 6 | 3 | 3 | 7 |
| 26.50-26.75 | 9 | 7 | 5 | 5 | 3 | 1 | 9 |
| 26.75-27.00 | 10 | 3 | 5 | 5 | 4 | 6 | 6 |
| 27.00-27.25 | 8 | 2 | 4 | 5 | 4 | 9 | 7 |
| 27.25-27.50 | 8 | 3 | 8 | 7 | 4 | 4 | 6 |
| 27.50-27.75 | 6 | 4 | 8 | 9 | 4 | 3 | 5 |
| 27.75-27.85 | 4 | 3 | 8 | 9 | 7 | 4 | 5 |
| 27.85-27.95 | 3 | 10 | 5 | 8 | 4 | 5 | 5 |
| 27.95-28.05 | 3 | 10 | 6 | 9 | 2 | 2 | 6 |
| 28.05-28.10 | 10 | 5 | 6 | 4 | 3 | 2 | 9 |
| 28.10-28.15 | 8 | 7 | 6 | 6 | 1 | 3 | 8 |
| 28.15-28.20 | 8 | 5 | 7 | 8 | 1 | 4 | 6 |
| >28.20 | 5 | 10 | 3 | 8 | 3 | 0 | 4 |
| *Indo-Pacific density intervals* | | | | | | | |
| <26.00 | 8 | 4 | 7 | 4 | 8 | 2 | 6 |
| 26.00-26.5 | 9 | 4 | 4 | 5 | 2 | 7 | 8 |
| 26.50-26.75 | 7 | 3 | 6 | 6 | 7 | 2 | 8 |
| 26.75-27.00 | 6 | 2 | 7 | 7 | 6 | 2 | 9 |
| 27.00-27.25 | 4 | 10 | 7 | 7 | 2 | 3 | 6 |
| 27.25-27.50 | 5 | 7 | 7 | 8 | 2 | 3 | 8 |
| 27.50-27.75 | 8 | 7 | 6 | 6 | 1 | 3 | 8 |
| 27.75-27.85 | 10 | 5 | 3 | 3 | 3 | 5 | 7 |
| 27.85-27.95 | 7 | 4 | 6 | 6 | 2 | 7 | 7 |
| 27.95-28.05 | 4 | 6 | 9 | 9 | 2 | 5 | 4 |
| 28.05-28.10 | 1 | 4 | 8 | 8 | 3 | 9 | 6 |
| >28.10 | 2 | 4 | 7 | 8 | 3 | 9 | 7 |

(a) Shown is number of times this variable is part of the 10 best MLR regressions

**Table S2.**

List of the sensitivity cases considered. V101 is the standard case.

| Identi–fier | Description | Number of regions | Number of iso slabs | Variables | Data source | Data mapping | Surface method |
|---|---|---|---|---|---|---|---|
| **101** | **Standard Case** | **2** | **14 + 12** | **all** | **GLODAP2+** | **WOA &GLODAP** | **combined** |
| 102 | only WOA (No GLODAP) | 2 | 14 + 12 | all | GLODAP2+ | WOA only | combined |
| 103 | no PO4* | 2 | 14 + 12 | all wo PO4* | GLODAP2+ | WOA &GLODAP2 | combined |
| 104 | Southern Ocean | 3 + S. Oce. | 14 + 12 | all | GLODAP2+ | WOA &GLODAP2 | combined |
| 105 | upper ocean: two regions; lower ocean: one region | 2+1 | 14 + 12 | all | GLODAP2+ | WOA &GLODAP2 | combined |
| 106 | only Carter variables† | 2 | 14 + 12 | Carter variables | GLODAP2+ | WOA &GLODAP2 | combined |
| 107 | 5 regions | 5 | 14 + 12 | all | GLODAP2+ | WOA &GLODAP2 | combined |
| 108 | no A16 2013 | 2+1 | 14 + 12 | all | GLODAP2 wo A16 | WOA &GLODAP2 | combined |
| 109 | reduced number isopycnal, 2 regions | 2 | 10 + 8 | all | GLODAP2+ | WOA &GLODAP2 | combined |
| 110 | reduced number isopycnal, 5 regions | 5 | 10 + 8 | all | GLODAP2+ | WOA &GLODAP2 | combined |
| 111 | no sfc equ | 2 | 14 + 12 | all | GLODAP2+ | WOA &GLODAP2 | eMLR only |
| 112 | global sfc equ | 2 | 14 + 12 | all | GLODAP2+ | WOA &GLODAP2 | surface equilibrium only |
| 113 | C* based on NO3 | 2 | 14 + 12 | all | GLODAP2+ | WOA &GLODAP2 | combined |
| 114 | all data GLODAP2 | 2 | 14 + 12 | all | GLODAP2 | WOA &GLODAP2 | combined |

† Only the variables used by Carter et al. (*43*) are used as predictors in the eMLRs.

**Table S3.**

Reconstructed column inventories (0-3000m) in the different ocean basins for each of the sensitivity cases listed in Table S2. Note that this table includes just the inventories for the regions mapped by the eMLR(C*) method, i.e., the numbers here neither include the Arctic and other marginal seas nor the ocean below 3000m.

| Version | North Atlantic (Pg C) | South Atlantic (Pg C) | North Pacific (Pg C) | South Pacific (Pg C) | Indian (Pg C) | Global (Pg C) |
|---|---|---|---|---|---|---|
| **101 (Std)** | **5.3** | **5.6** | **5.2** | **8.0** | **7.1** | **31.2** |
| 102 | 5.2 | 5.0 | 5.8 | 8.7 | 6.7 | 31.4 |
| 103 | 5.3 | 5.5 | 5.0 | 8.0 | 6.4 | 30.1 |
| 104 | 5.5 | 5.1 | 4.6 | 8.6 | 8.0 | 31.9 |
| 105 | 5.1 | 4.8 | 6.6 | 10.1 | 8.7 | 35.3 |
| 106 | 5.5 | 6.3 | 6.5 | 9.3 | 9.3 | 36.9 |
| 107 | 5.3 | 4.7 | 5.4 | 8.5 | 9.7 | 33.5 |
| 108 | 5.1 | 5.4 | 5.3 | 8.0 | 6.9 | 30.7 |
| 109 | 5.4 | 5.4 | 5.3 | 8.1 | 7.0 | 31.2 |
| 110 | 5.4 | 4.7 | 5.4 | 8.4 | 9.4 | 33.2 |
| 111 | 5.5 | 5.4 | 5.3 | 7.9 | 6.4 | 30.5 |
| 112 | 5.4 | 5.6 | 5.3 | 8.2 | 7.3 | 31.7 |
| 113 | 5.4 | 5.6 | 5.3 | 8.2 | 6.8 | 31.3 |
| 114 | 4.7 | 5.5 | 5.1 | 7.8 | 6.5 | 29.6 |
| **Median** | **5.3** | **5.4** | **5.3** | **8.2** | **7.0** | **31.3** |
| **IQR** | **0.2** | **0.5** | **0.2** | **0.6** | **1.8** | **2.0** |

**References and Notes**


1. C. L. Sabine *et al*., The oceanic sink for anthropogenic $CO_2$. *Science* **305**, 367–371 (2004).

2. B. I. McNeil, R. J. Matear, The non-steady state oceanic $CO_2$ signal: Its importance, magnitude and a novel way to detect it. *Biogeosciences* **10**, 2219–2228 (2013). doi:10.5194/bg-10-2219-2013

3. J. L. Sarmiento, J. C. Orr, U. Siegenthaler, A perturbation Simulation of $CO_2$ uptake in an Ocean General Circulation Model. *J. Geophys. Res.* **97** (C3), 3621–3645 (1992). doi:10.1029/91JC02849

4. R. A. Houghton, A. A. Nassikas, Global and regional fluxes of carbon from land use and land cover change 1850–2015. *Global Biogeochem. Cycles* **31**, 456–472 (2017). doi:10.1002/2016GB005546

5. T. Boden, G. Marland, R. J. Andres, (1999): Global, Regional, and National Fossil-Fuel $CO_2$ Emissions (1751 - 2014) (V. 2017) (Carbon Dioxide Information Analysis Center, Oak Ridge National Laboratory, Oak Ridge, TN). doi:10.3334/CDIAC/00001_V2017

6. N. Gruber, M. Gloor, S. E. Mikaloff Fletcher, S. C. Doney, S. Dutkiewicz, M. J. Follows, M. Gerber, A. R. Jacobson, F. Joos, K. Lindsay, D. Menemenlis, A. Mouchet, S. A. Müller, J. L. Sarmiento, T. Takahashi, Oceanic sources, sinks, and transport of atmospheric $CO_2$. *Global Biogeochem. Cycles* **23**, GB1005 (2009). doi:10.1029/2008GB003349

7. L. D. Talley, R. A. Feely, B. M. Sloyan, R. Wanninkhof, M. O. Baringer, J. L. Bullister, C. A. Carlson, S. C. Doney, R. A. Fine, E. Firing, N. Gruber, D. A. Hansell, M. Ishii, G. C. Johnson, K. Katsumata, R. M. Key, M. Kramp, C. Langdon, A. M. Macdonald, J. T. Mathis, E. L. McDonagh, S. Mecking, F. J. Millero, C. W. Mordy, T. Nakano, C. L. Sabine, W. M. Smethie, J. H. Swift, T. Tanhua, A. M. Thurnherr, M. J. Warner, J.-Z. Zhang, Changes in Ocean Heat, Carbon Content, and Ventilation: A Review of the First Decade of GO-SHIP Global Repeat Hydrography. *Annu. Rev. Mar. Sci.* **8**, 185–215 (2016). doi:10.1146/annurev-marine-052915-100829 Medline

8. A. Olsen, R. M. Key, S. van Heuven, S. K. Lauvset, A. Velo, X. Lin, C. Schirnick, A. Kozyr, T. Tanhua, M. Hoppema, S. Jutterström, R. Steinfeldt, E. Jeansson, M. Ishii, F. F. Pérez, T. Suzuki, The Global Ocean Data Analysis Project version 2 (GLODAPv2) – an internally consistent data product for the world ocean. *Earth Syst. Sci. Data* **8**, 297–323 (2016). doi:10.5194/essd-8-297-2016

9. D. Clement, N. Gruber, The eMLR(C*) Method to Determine Decadal Changes in the Global Ocean Storage of Anthropogenic $CO_2$. *Global Biogeochem. Cycles* **32**, 654–679 (2018). doi:10.1002/2017GB005819

10. K. Friis, A. Körtzinger, J. Pätsch, D. W. R. Wallace, On the temporal increase of anthropogenic $CO_2$ in the subpolar North Atlantic. *Deep. Res. Part I.* **52**, 681–698 (2005). doi:10.1016/j.dsr.2004.11.017

11. J. L. Sarmiento, N. Gruber, *Ocean Biogeochemical Dynamics* (Princeton Univ. Press, Princeton, NJ, 2006).

12. N. Gruber, Anthropogenic $CO_2$ in the Atlantic Ocean. *Global Biogeochem. Cycles* **12**, 165–191 (1998). doi:10.1029/97GB03658

13. S. Khatiwala, T. Tanhua, S. Mikaloff Fletcher, M. Gerber, S. C. Doney, H. D. Graven, N. Gruber, G. A. McKinley, A. Murata, A. F. Ríos, C. L. Sabine, Global ocean storage of anthropogenic carbon. *Biogeosciences* **10**, 2169–2191 (2013). doi:10.5194/bg-10-2169-2013

14. T. DeVries, The oceanic anthropogenic $CO_2$ sink: Storage, air-sea fluxes, and transports over the industrial era. *Global Biogeochem. Cycles* **28**, 631–647 (2014). doi:10.1002/2013GB004739

15. D. R. Jackett, T. J. McDougall, A Neutral Density Variable for the World's Oceans. *J. Phys. Oceanogr.* **27**, 237–263 (1997). doi:10.1175/1520-0485(1997)027<0237:ANDVFT>2.0.CO;2

16. K. Hanawa, L. D. Talley, in *Ocean Circulation and Climate*, G. Siedler, J. Church, Eds. (Academic Press, San Diego, 2001), pp. 373–386.

17. S. E. Mikaloff Fletcher, N. Gruber, A. R. Jacobson, S. C. Doney, S. Dutkiewicz, M. Gerber, M. Follows, F. Joos, K. Lindsay, D. Menemenlis, A. Mouchet, S. A. Müller, J. L. Sarmiento, Inverse estimates of anthropogenic $CO_2$ uptake, transport, and storage by the ocean. *Global Biogeochem. Cycles* **20**, GB2002 (2006). doi:10.1029/2005GB002530

18. L. Bopp, M. Lévy, L. Resplandy, J. B. Sallée, Pathways of anthropogenic carbon subduction in the global ocean. *Geophys. Res. Lett.* **42**, 6416–6423 (2015). doi:10.1002/2015GL065073

19. J. Marshall, K. Speer, Closure of the meridional overturning circulation through Southern Ocean upwelling. *Nat. Geosci.* **5**, 171–180 (2012). doi:10.1038/ngeo1391

20. M. Hoppema, W. Roether, R. G. J. Bellerby, H. J. W. de Baar, Direct measurements reveal insignificant storage of anthropogenic $CO_2$ in the Abyssal Weddell Sea. *Geophys. Res. Lett.* **28**, 1747–1750 (2001). doi:10.1029/2000GL012443

21. T. DeVries, M. Holzer, F. Primeau, Recent increase in oceanic carbon uptake driven by weaker upper-ocean overturning. *Nature* **542**, 215–218 (2017). doi:10.1038/nature21068 Medline

22. A. Olsen, A. M. Omar, E. Jeansson, L. G. Anderson, R. G. J. Bellerby, Nordic seas transit time distributions and anthropogenic $CO_2$. *J. Geophys. Res.* **115**, C05005 (2010). doi:10.1029/2009JC005488

23. T. Tanhua, E. P. Jones, E. Jeansson, S. Jutterström, W. M. Smethie Jr., D. W. R. Wallace, L. G. Anderson, Ventilation of the Arctic Ocean: Mean ages and inventories of anthropogenic $CO_2$ and CFC-11. *J. Geophys. Res.* **114**, C01002 (2009). doi:10.1029/2008JC004868

24. A. Schneider, T. Tanhua, A. Körtzinger, D. W. R. Wallace, High anthropogenic carbon content in the eastern Mediterranean. *J. Geophys. Res.* **115**, C12050 (2010). doi:10.1029/2010JC006171

25. R. Wanninkhof, G.-H. Park, T. Takahashi, R. A. Feely, J. L. Bullister, S. C. Doney, Changes in deep-water $CO_2$ concentrations over the last several decades determined from discrete $pCO_2$ measurements. *Deep Sea Res. Part II Top. Stud. Oceanogr.* **74**, 48–63 (2013). doi:10.1016/j.dsr.2012.12.005

26. S. Khatiwala, F. Primeau, T. Hall, Reconstruction of the history of anthropogenic $CO(_2)$ concentrations in the ocean. *Nature* **462**, 346–349 (2009). doi:10.1038/nature08526 Medline

27. R. H. Gammon, J. Cline, D. Wisegarver, Chlorofluoromethanes in the Northeast Pacific Ocean: Measured vertical distributions and application as transient tracers of upper ocean mixing. *J. Geophys. Res.* **87** (C12), 9441–9454 (1982). doi:10.1029/JC087iC12p09441

28. T. Tanhua, A. Körtzinger, K. Friis, D. W. Waugh, D. W. R. Wallace, An estimate of anthropogenic $CO_2$ inventory from decadal changes in oceanic carbon content. *Proc. Natl. Acad. Sci. U.S.A.* **104**, 3037–3042 (2007). doi:10.1073/pnas.0606574104 Medline

29. R. Steinfeldt, M. Rhein, J. L. Bullister, T. Tanhua, Inventory changes in anthropogenic carbon from 1997–2003 in the Atlantic Ocean between 20°S and 65°N. *Global Biogeochem. Cycles* **23**, GB3010 (2009). doi:10.1029/2008GB003311

30. R. Wanninkhof, S. C. Doney, J. L. Bullister, N. M. Levine, M. Warner, N. Gruber, Detecting anthropogenic $CO_2$ changes in the interior Atlantic Ocean between 1989 and 2005. *J. Geophys. Res.* **115**, C11028 (2010). doi:10.1029/2010JC006251

31. F. F. Pérez, H. Mercier, M. Vázquez-Rodríguez, P. Lherminier, A. Velo, P. C. Pardo, G. Rosón, A. F. Ríos, Atlantic Ocean $CO_2$ uptake reduced by weakening of the meridional overturning circulation. *Nat. Geosci.* **6**, 146–152 (2013). doi:10.1038/ngeo1680

32. F. Fröb, A. Olsen, K. Våge, G. W. K. Moore, I. Yashayaev, E. Jeansson, B. Rajasakaren, Irminger Sea deep convection injects oxygen and anthropogenic carbon to the ocean interior. *Nat. Commun.* **7**, 13244 (2016). doi:10.1038/ncomms13244 Medline

33. D. W. J. Thompson, S. Solomon, Interpretation of recent Southern Hemisphere climate change. *Science* **296**, 895–899 (2002). doi:10.1126/science.1069270 Medline

34. D. W. Waugh, F. Primeau, T. Devries, M. Holzer, Recent Changes in the Ventilation of the Southern Oceans. *Science* **339**, 568–570 (2013).

35. T. Tanhua, M. Hoppema, E. M. Jones, T. Stöven, J. Hauck, M. G. Dávila, M. Santana-Casiano, M. Álvarez, V. H. Strass, Temporal changes in ventilation and

the carbonate system in the Atlantic sector of the Southern Ocean. *Deep-Sea Res. Part II Top. Stud. Oceanogr.* **138**, 26–38 (2017). doi:10.1016/j.dsr2.2016.10.004

36. C. Le Quéré, R. M. Andrew, P. Friedlingstein, S. Sitch, J. Pongratz, A. C. Manning, J. I. Korsbakken, G. P. Peters, J. G. Canadell, R. B. Jackson, T. A. Boden, P. P. Tans, O. D. Andrews, V. K. Arora, D. C. E. Bakker, L. Barbero, M. Becker, R. A. Betts, L. Bopp, F. Chevallier, L. P. Chini, P. Ciais, C. E. Cosca, J. Cross, K. Currie, T. Gasser, I. Harris, J. Hauck, V. Haverd, R. A. Houghton, C. W. Hunt, G. Hurtt, T. Ilyina, A. K. Jain, E. Kato, M. Kautz, R. F. Keeling, K. Klein Goldewijk, A. Körtzinger, P. Landschützer, N. Lefèvre, A. Lenton, S. Lienert, I. Lima, D. Lombardozzi, N. Metzl, F. Millero, P. M. S. Monteiro, D. R. Munro, J. E. M. S. Nabel, S. Nakaoka, Y. Nojiri, X. A. Padin, A. Peregon, B. Pfeil, D. Pierrot, B. Poulter, G. Rehder, J. Reimer, C. Rödenbeck, J. Schwinger, R. Séférian, I. Skjelvan, B. D. Stocker, H. Tian, B. Tilbrook, F. N. Tubiello, I. T. van der Laan-Luijkx, G. R. van der Werf, S. van Heuven, N. Viovy, N. Vuichard, A. P. Walker, A. J. Watson, A. J. Wiltshire, S. Zaehle, D. Zhu, Global Carbon Budget 2017. *Earth Syst. Sci. Data* **10**, 405–448 (2018). doi:10.5194/essd-10-405-2018

37. E. Dlugokencky, P. Tans, "Trends in atmospheric carbon dioxide" (Boulder, CO, USA, 2017); www.esrl.noaa.gov/gmd/ccgg/trends/gl_data.html.

38. R. F. Keeling, Comment on "The Ocean Sink for Anthropogenic $CO_2$.". *Science* **308**, 1743c (2005). doi:10.1126/science.1109620

39. P. Landschützer, N. Gruber, D. C. E. Bakker, Decadal variations and trends of the global ocean carbon sink. *Global Biogeochem. Cycles* **30**, 1396–1417 (2016). doi:10.1002/2015GB005359

40. S. C. Doney, V. J. Fabry, R. A. Feely, J. A. Kleypas, Ocean acidification: The other $CO_2$ problem. *Annu. Rev. Mar. Sci.* **1**, 169–192 (2009). doi:10.1146/annurev.marine.010908.163834 Medline

41. R. A. Feely, C. L. Sabine, K. Lee, W. Berelson, J. Kleypas, V. J. Fabry, F. J. Millero, Impact of Anthropogenic $CO_2$ on the $CaCO_3$ System in the Oceans. *Science* **305**, 362–366 (2004). doi:10.1126/science.1097329

42. F. F. Perez, M. Fontela, M. I. García-Ibáñez, H. Mercier, A. Velo, P. Lherminier, P. Zunino, M. de la Paz, F. Alonso-Pérez, E. F. Guallart, X. A. Padin, Meridional overturning circulation conveys fast acidification to the deep Atlantic Ocean. *Nature* **554**, 515–518 (2018). doi:10.1038/nature25493 Medline

43. B. R. Carter, R. A. Feely, S. Mecking, J. N. Cross, A. M. Macdonald, S. A. Siedlecki, L. D. Talley, C. L. Sabine, F. J. Millero, J. H. Swift, A. G. Dickson, K. B. Rodgers, Two decades of Pacific anthropogenic carbon storage and ocean acidification along Global Ocean Ship-based Hydrographic Investigations Program sections P16 and P02. *Global Biogeochem. Cycles* **31**, 306–327 (2017). doi:10.1002/2016GB005485

44. K. J. Kroeker, R. L. Kordas, R. N. Crim, G. G. Singh, Meta-analysis reveals negative yet variable effects of ocean acidification on marine organisms. *Ecol. Lett.* **13**, 1419–1434 (2010). doi:10.1111/j.1461-0248.2010.01518.x Medline

45. N. Gruber, J. L. Sarmiento, T. F. Stocker, An improved method for detecting anthropogenic $CO_2$ in the oceans. *Global Biogeochem. Cycles* **10**, 809–837 (1996). doi:10.1029/96GB01608

46. P. Regnier, P. Friedlingstein, P. Ciais, F. T. Mackenzie, N. Gruber, I. A. Janssens, G. G. Laruelle, R. Lauerwald, S. Luyssaert, A. J. Andersson, S. Arndt, C. Arnosti, A. V. Borges, A. W. Dale, A. Gallego-Sala, Y. Goddéris, N. Goossens, J. Hartmann, C. Heinze, T. Ilyina, F. Joos, D. E. LaRowe, J. Leifeld, F. J. R. Meysman, G. Munhoven, P. A. Raymond, R. Spahni, P. Suntharalingam, M. Thullner, Anthropogenic perturbation of the carbon fluxes from land to ocean. *Nat. Geosci.* **6**, 597–607 (2013). doi:10.1038/ngeo1830

47. C. Sabine, N. Gruber, Response to Comment on "The Ocean Sink for Anthropogenic $CO_2$". *Science* **308**, 1743d (2005). doi:10.1126/science.1109949

48. E. Hansis, S. J. Davis, J. Pongratz, Relevance of methodological choices for accounting of land use change carbon fluxes. *Global Biogeochem. Cycles* **29**, 1230–1246 (2015). doi:10.1002/2014GB004997

49. R. M. Key, A. Kozyr, C. L. Sabine, K. Lee, R. Wanninkhof, J. L. Bullister, R. A. Feely, F. J. Millero, C. Mordy, T.-H. Peng, A global ocean carbon climatology: Results from Global Data Analysis Project (GLODAP). *Global Biogeochem. Cycles* **18**, GB4031 (2004). doi:10.1029/2004GB002247

50. T. Tanhua, R. Steinfeldt, R. M. Key, P. Brown, N. Gruber, R. Wanninkhof, F. Perez, A. Körtzinger, A. Velo, U. Schuster, S. van Heuven, J. L. Bullister, I. Stendardo, M. Hoppema, A. Olsen, A. Kozyr, D. Pierrot, C. Schirnick, D. W. R. Wallace, Atlantic Ocean CARINA data : Overview and salinity adjustments. *Earth Syst. Sci. Data* **2**, 17–34 (2010). doi:10.5194/essd-2-17-2010

51. R. M. Key, T. Tanhua, A. Olsen, M. Hoppema, S. Jutterström, C. Schirnick, S. van Heuven, A. Kozyr, X. Lin, A. Velo, D. W. R. Wallace, L. Mintrop, The CARINA data synthesis project: Introduction and overview. *Earth Syst. Sci. Data* **2**, 105–121 (2010). doi:10.5194/essd-2-105-2010

52. K. Suzuki, T., Ishii, M., Aoyama, A., Christian, J. R., Enyo, L. A. Kawano, T., Key, R. M., Kosugi, N., Kozyr, A., Miller, S. Murata, A., Nakano, T., Ono, T., Saino, T., Sasaki, K., C. L. D., Takatani, Y., Wakita, M., and Sabine, "PACIFICA Data Synthesis Project" (2013), doi:10.3334/CDIAC/OTG.PACIFICA_NDP092.

53. S. K. Lauvset, R. M. Key, A. Olsen, S. van Heuven, A. Velo, X. Lin, C. Schirnick, A. Kozyr, T. Tanhua, M. Hoppema, S. Jutterström, R. Steinfeldt, E. Jeansson, M. Ishii, F. F. Perez, T. Suzuki, S. Watelet, A new global interior ocean mapped climatology: The 1°x1° GLODAP version 2. *Earth Syst. Sci. Data* **8**, 325–340 (2016). doi:10.5194/essd-8-325-2016

54. R. A. Locarnini *et al.*, *World Ocean Atlas 2013, Volume 1: Temperature* (NOAA, 2013).

55. M. M. Weng *et al.*, *World Ocean Atlas 2013: Volume 2: Salinity* (NOAA, 2013).

56. M. Aoyama, H. Ota, M. Kimura, T. Kitao, H. Mitsuda, A. Murata, K. Sato, Current Status of Homogeneity and Stability of the Reference Materials for Nutrients in Seawater. *Anal. Sci.* **28**, 911–916 (2012). doi:10.2116/analsci.28.911

57. R. E. Sonnerup, P. D. Quay, A. P. McNichol, The Indian Ocean $^{13}C$ Suess Effect. *Global Biogeochem. Cycles* **14**, 903–916 (2000). doi:10.1029/1999GB001244

58. Y. Plancherel, K. B. Rodgers, R. M. Key, R. Jacobson, J. L. Sarmiento, Role of regression model selection and station distribution on the estimation of oceanic anthropogenic carbon change by eMLR. *Biogeosciences* **10**, 4801–4831 (2013). doi:10.5194/bg-10-4801-2013

59. N. Gruber, J. L. Sarmiento, in *THE SEA: Biological-Physical Interactions in the Oceans*, A. R. Robinson, J. J. McCarthy, B. J. Rothschild, Eds. (Wiley, New York, 2002), vol. 12, pp. 337–399.

60. A. C. Martiny, C. T. A. Pham, F. W. Primeau, J. A. Vrugt, J. K. Moore, S. A. Levin, M. W. Lomas, Strong latitudinal patterns in the elemental ratios of marine plankton and organic matter. *Nat. Geosci.* **6**, 279–283 (2013). doi:10.1038/ngeo1757

61. R. J. Woosley, F. J. Millero, R. Wanninkhof, Rapid anthropogenic changes in $CO_2$ and pH in the Atlantic Ocean: 2003-2014. *Global Biogeochem. Cycles* **30**, 70–90 (2016). doi:10.1002/2015GB005248

62. W. S. Broecker, S. Blanton, W. M. Smethie Jr., G. Ostlund, Radiocarbon decay and oxygen utilization in the deep Atlantic Ocean. *Global Biogeochem. Cycles* **5**, 87–117 (1991). doi:10.1029/90GB02279

63. B. I. McNeil, R. J. Matear, R. M. Key, J. L. Bullister, J. L. Sarmiento, Anthropogenic $CO_2$ Uptake by the Ocean Based on the Global Chlorofluorocarbon Data Set. *Science* **299**, 235–239 (2003).

64. S. van Heuven, D. Pierrot, J. W. B. Rae, E. Lewis, D. W. R. Wallace, MATLAB Program Developed for $CO_2$ System Calculations (2011). doi:10.3334/CDIAC/otg.CO2SYS_MATLAB_v1.1.

65. C. Mehrbach, C. H. Culberson, J. E. Hawley, R. M. Pytkowicx, Measurement of the apparent dissociation constants of carbonic acid in seawater at atmospheric pressure. *Limnol. Oceanogr.* **18**, 897–907 (1973). doi:10.4319/lo.1973.18.6.0897

66. A. G. Dickson, F. J. Millero, A comparison of the equilibrium constants for the dissociation of carbonic acid in seawater media. *Deep-Sea Res.* **34**, 1733–1743 (1987). doi:10.1016/0198-0149(87)90021-5

67. S. Kouketsu, A. M. Murata, Detecting decadal scale increases in anthropogenic $CO_2$ in the ocean. *Geophys. Res. Lett.* **41**, 4594–4600 (2014). doi:10.1002/2014GL060516

68. J. L. Sarmiento, C. LeQuéré, S. W. Pacala, Limiting future atmospheric carbon dioxide. *Global Biogeochem. Cycles* **9**, 121–137 (1995). doi:10.1029/94GB01779

69. K. Matsumoto, N. Gruber, How accurate is the estimation of anthropogenic carbon in the ocean? An evaluation of the ΔC* method. *Global Biogeochem. Cycles* **19**, (2005). doi:10.1029/2004GB002397

70. L. Resplandy, R. F. Keeling, C. Rödenbeck, B. B. Stephens, S. Khatiwala, K. B. Rodgers, M. C. Long, L. Bopp, P. P. Tans, Revision of global carbon fluxes based on a reassessment of oceanic and riverine carbon transport. *Nat. Geosci.* **11**, 504–509 (2018). doi:10.1038/s41561-018-0151-3

71. A. R. Jacobson, S. E. Mikaloff Fletcher, N. Gruber, J. L. Sarmiento, M. Gloor, A joint atmosphere-ocean inversion for surface fluxes of carbon dioxide: 1. Methods and global-scale fluxes. *Global Biogeochem. Cycles* **21**, 1–13 (2007).